Interaction Mechanism of Re(VII) with Zirconium Dioxide Nanoparticles Archored onto Reduced Graphene Oxides

Yang Gao,[†,‡] Ke Chen,[†] Xiaoli Tan,*[,†] Xianlong Wang,[⊥] Ahmed Alsaedi,[§] Tasawar Hayat,*[,§,∥] and Changlun Chen*[,†,‡,§]

[†]Institute of Plasma Physics, Chinese Academy of Sciences, P.O. Box 1126, Hefei 230031, P.R. China

[‡]Collaborative Innovation Center of Radiation Medicine of Jiangsu Higher Education Institutions, Soochow University, Suzhou 215123, P.R. China

[§]NAAM Research Group, Faculty of Science, King Abdulaziz University, Jeddah 21589, Saudi Arabia

[∥]Department of Mathematics, Quaid-I-Azam University, Islamabad 44000, Pakistan

[⊥]Institute of Solid States Physics, Chinese Academy of Sciences, P.O. Box 1129, Hefei 230031, P.R. China

S *Supporting Information*

ABSTRACT: Zirconium oxide archored onto reduced graphene oxides (ZrO$_2$@rGO) was fabricated via a hydrothermal method and used for Re(VII) removal from aqueous solutions. Scanning electron microscopy, Fourier transferred infrared spectroscopy, X-ray diffraction, thermogravimetric analysis, and X-ray photoelectron spectroscopy were used to characterize the as-prepared ZrO$_2$@rGO. The results indicated that ZrO$_2$ was successfully decorated on rGO. The maximum sorption capacity of ZrO$_2$@rGO toward Re(VII) was 43.55 mg/g. ZrO$_2$@rGO exhibited enhanced sorption capacity for Re(VII) in comparison with bare ZrO$_2$ or rGO. The sorption kinetics could be described by the pseudo-second-order equation. The sorption process of Re(VII) on ZrO$_2$@rGO was endothermic and spontaneous. X-ray photoelectron spectroscopy indicated the formation of an ionic bond of Zr−O with Re(VII). According to the density functional theory calculations, O$_{Re}$−Zr bonds on the surface of the monoclinic ZrO$_2$ plane (m-ZrO$_2$) (111) plane and tetragonal ZrO$_2$ (t-ZrO$_2$) (111) plane were formed when Re(VII) sorbs. The sorption energy of Re(VII) onto the t-ZrO$_2$ (111) plane was 3.87 eV, being higher than that of Re(VII) onto m-ZrO$_2$ (1.26 eV).

KEYWORDS: *ZrO$_2$@rGO, Sorption, Re(VII), Interaction mechanism*
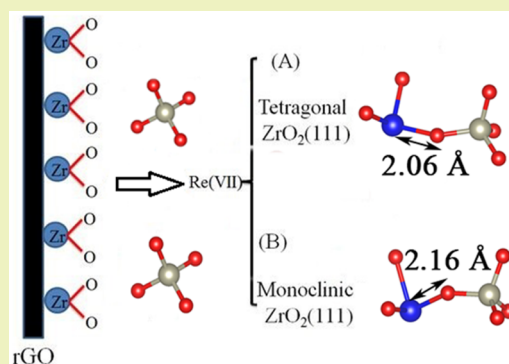
INTRODUCTION

Technetium-99 (Tc^{99}) is the byproduct of U^{235} fission in nuclear reactors. Tc^{99} decays via β emission, presenting internal radiological hazards to internal organs and external hazards to the skin.[1−3] Radioactive element ^{99}Tc exists in the most thermodynamically steady heptavalent pertechnetate anion (TcO$_4^-$) predominantly.[1] Once the groundwater is contaminated by radionuclide waste, TcO$_4^-$ can diffuse through soil very easily.[4−6] Therefore, a promising efficient approach for the treatment of Tc(VII)-contaminated waste is necessary. Tc is only available in limited quantities as man-made, radioactive isotopes. Therefore, a more readily available and nonradioactive surrogate of ^{99}Tc is needed to emulate its chemical and sorption behavior. One of the most important promising candidates for a Tc surrogate is Re.[7−9] Re in the periodic table was selected as an attractive surrogate for Tc due to the proximities of Tc with Re based on the first-principles basis.[4] The most stable oxidation state of the Re and Tc species is +7 in solution or solid state. The main forms of Re and Tc are ReO$_4^-$ and TcO$_4^-$ anions in aqueous environments almost over the entire pH range from 0 to 14.[4] Therefore, we chose Re (nonradioactive metal element) to simulate the chemical and physical properties of radioactive element ^{99}Tc.

There are some reports on the removal of Re(VII), including modified nano-Al$_2$O$_3$, NZVI, PANI, modified brown algae, orange peel (Zr(VI)-loaded), and persimmon (formaldehyde).[5−12] However, the sorption capacities of these materials were very low. Therefore, it is important to develop novel high capacity sorbents for Re(VII) removal.

The hydrothermal method is a simple, convenient, and economical method to modify inorganic materials (interchangeable). All one needs to do is add these materials or their precursors into a Teflon-lined stainless steel autoclave to prepare organic−inorganic hybrid materials. Organic−inorganic hybrid materials have drawn wide attention for removing heavy metal ions.[13] Organic−inorganic hybrid materials show several remarkable and amazing properties, e.g., a very large surface area to volume ratio and flexibility in surface functionalities, as
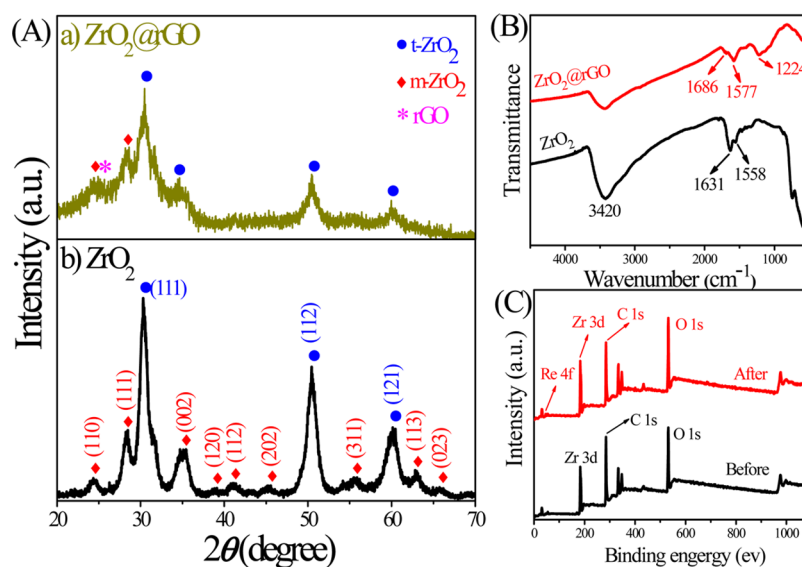
Figure 1. (A) XRD patterns of (a) ZrO$_2$@rGO and (b) particles of ZrO$_2$. (B) FT-IR spectra of ZrO$_2$@rGO(90:800) and particles of ZrO$_2$. (C) XPS characterization of ZrO$_2$@rGO before and after Re(VII) sorption.

well as superior mechanical performance.[14−16] Zirconium oxide (ZrO$_2$) is an inorganic material that has been widely used as a sorbent because it is nontoxic, chemically inert, and insoluble in water.[17−25] Hristovski et al.[18] used ZrO$_2$ as a sorbent to remove As(V). Rodrigues et al.[20] reported Cr(VI) removal from an aqueous solution by hydrous ZrO$_2$. Luo et al.[21] used ZrO$_2$ to remove Sb(V) and Sb(III). Cui et al.[22] used nanostructured ZrO$_2$ spheres for a fixed bed reactor to simultaneously remove As(V) and As(III).

In the present work, ZrO$_2$ particles were decorated on the surface of reduced GOs (denoted by ZrO$_2$@rGO) by a hydrothermal method. Scanning electron microscopy (SEM), X-ray diffraction, photoelectron spectroscopy (XRD and XPS), Fourier transform infrared spectroscopy (FT-IR), thermogravimetric analysis (TGA), and zeta-potential measurements are used to characterize ZrO$_2$@rGO. The anion Re(VII) sorption on ZrO$_2$@rGO was studied using the change in shaking time, pH, ionic strength, and temperature in batch experiments. We proposed a possible removal mechanism for Re(VII) using X-ray photoelectron spectroscopy (XPS) and density functional theory (DFT) calculations. We demonstrated that ZrO$_2$@rGO was a promising candidate for Re(VII) removal.

■ EXPERIMENTAL SECTION

Chemicals. All chemicals were analytical purity grade without further treatment. All water in this experiment is Milli-Q (Milli-pore, Billerica, MA, U.S.A.). Re(VII) stock solution (1.0 mmol/L) was prepared by dissolving NaReO$_4$ in Milli-Q water.

Preparation of ZrO$_2$@rGO. A simple hydrothermal method was used to prepare ZrO$_2$@rGO. The modified Hummer's method was used to prepare GOs.[26] First, 90 mg of GO was dispersed in 50 mL of isopropanol and then sonicated for 30 min before adding up to 800 mg of ZrOCl$_2$·8H$_2$O. Subsequently, 5 mL of NaOH solution was dripped into the above mixture and stirred for 2 h at room temperature. After that, the mixture was transferred into a 100 mL Teflon-lined autoclave and maintained at 180 °C for 16 h. The obtained sample was washed with Milli-Q water and ethanol repeatedly. Finally, the prepared sample was dried by vacuum freeze-drying (−60 °C) for about 12 h. As a comparison, ZrO$_2$@rGO composites with the mass ratios of ZrO$_2$ to GO (200:90, 400:90, 1600:90) were synthesized the same way.

Characterization and sorption experiments are described in the Supporting Information.

Theoretical Interatomic Sorption Analysis by DFT. All the calculations based on DFT were carried out using Vienna Ab initio Simulation Package code,[27,28] using the projected-augmented-wave potential (PAW) method.[29,30] General gradient approximation calculations were carried out by using the exchange-correlation functional parametrized.[31] The valence states of $2s^2 2p^4$ of O, $5f^{14} 5d^5 6s^2$ of Re, and $4d^2 5s^2$ of Zr were included in the PAW potentials.The convergence of plane-wave expansion was obtained with a cutoff energy of 400 eV. The monoclinic ZrO$_2$ (m-ZrO$_2$) and tetragonal ZrO$_2$ (t-ZrO$_2$) surface on (111) planes were represented by a slab in a (2×2) supercell, and the model bottom was fixed with a 15 Å vacuum layer. The k-point meshes in the Brillouin zone (BZ) were sampled by $4 \times 4 \times 2$. All structures were optimized to the forces on all unconstrained atoms less than 0.01 eV/Å.

The adsorption energy (E_{ad}) of the Re(VII) molecule was calculated as

$$E_{ad} = E_{surface} + E_{Re} - E_{Re/surface} \qquad (1)$$

where $E_{surface}$ is the surface energy, E_{Re} is the Re(VII) molecule energy, and $E_{Re/surface}$ is the total energy of the Re(VII) molecule sorbed on the surface. A positive E_{ad} value implies a stable sorption.

■ RESULTS AND DISCUSSION

Characterization of ZrO$_2$, rGO, and ZrO$_2$@rGO. Figure S1A shows that the rGO sheets are smooth and delicate, and the sheets have a slight wrinkled-layer structure. Figure S1B shows that ZrO$_2$ is irregularly particles. Figure S1C shows that ZrO$_2$@rGO is cracked and coarse on the surface. It is evident that ZrO$_2$ is homogeneously aggregated and embedded on the rGO sheets.

The XRD patterns of ZrO$_2$@rGO and pure ZrO$_2$ particles are shown in Figure 1A. It is evident that ZrO$_2$ is the t-ZrO$_2$ and m-ZrO$_2$ mixture phases in the pure ZrO$_2$ particles (according to PDF 37-1484). After ZrO$_2$ was doped into rGO, the tetragonal ZrO$_2$ plane (t-ZrO$_2$) was the predominant phase (according to PDF 42-1164). The reduction of most m-ZrO$_2$ peaks of ZrO$_2$@rGO demonstrates that the ZrO$_2$ nanoparticles are dispersed on the surface of rGO nanosheets and do not aggregate into well-formed large crystal sizes for strong sharp XRD peaks.[21] The dramatic attenuation or disappearance of ZrO$_2$'s m-ZrO$_2$ characteristic peak in ZrO$_2$@rGO may contribute to stacking of rGO nanosheets
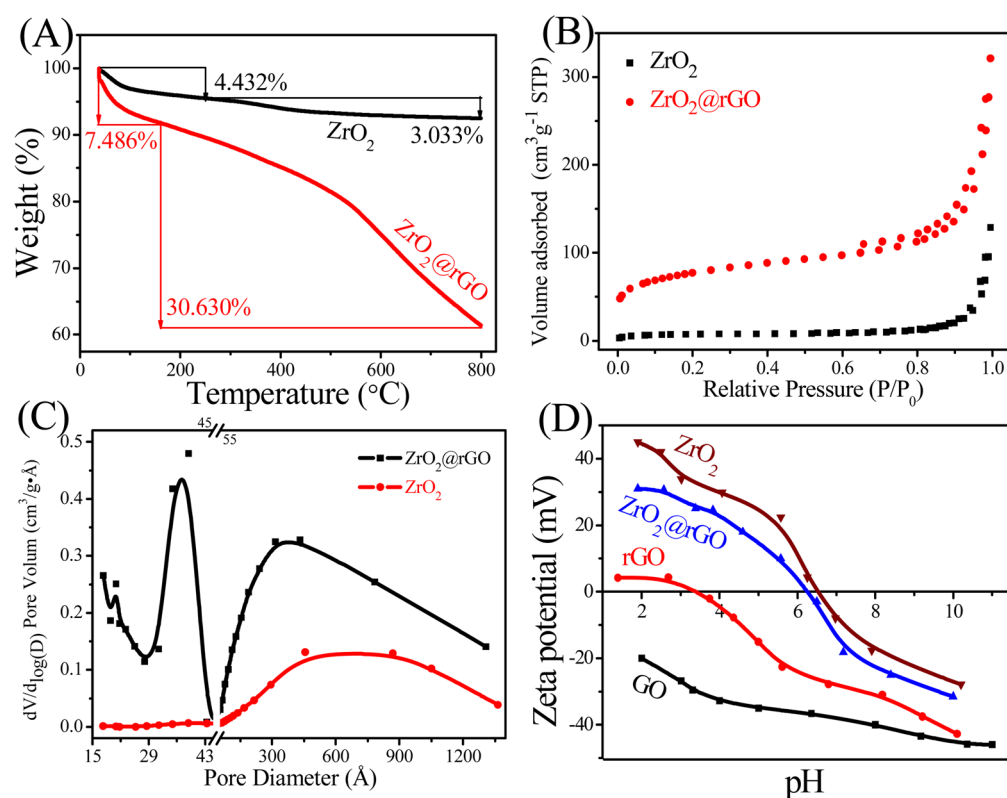
Figure 2. (A) TGA curves of ZrO$_2$ and ZrO$_2$@rGO. (B) N$_2$ adsorption−desorption isotherms of ZrO$_2$ and ZrO$_2$@rGO. (C) Distributions of pore diameter of ZrO$_2$ and ZrO$_2$@rGO. (D) Zeta potentials of GO, rGO, ZrO$_2$@rGO (90:800), and particles of ZrO$_2$ vs pH. Here, m/V = 0.1 g/L and I = 0.01 mol/L NaNO$_3$.

or incorporation of ZrO$_2$@rGO into the composites. Although the intensity in different materials of ZrO$_2$ between t-ZrO$_2$ and m-ZrO$_2$ is changing, the most distinctive peak near the 2θ angle of ∼30.4° is typical of a t-ZrO$_2$ structure zirconia and is still present. In the XRD patterns of ZrO$_2$@rGO, there is an unimpressive peak at 2θ = 26°, representing the characteristic peak of rGO, which makes a small peak at 2θ = 24.34° in ZrO$_2$ become stranger and broader in ZrO$_2$@rGO. Figure S2 shows the XRD patterns of GO (used as the original material in our experiment) and rGO nanosheets. The peaks of 9.02° and 26° are the characteristic peaks of GO and rGO, respectively.

The FT-IR spectra of GO and rGO are presented in Figure S3. The absorption peaks at 1735, 1625, 1385, 1227, and 1081 cm^{-1} in the FT-IR spectrum of GO are due to C=O, aromatic C=C, carboxyl O=C−O, epoxy C−O, and alkoxy C−O stretching vibrations, respectively. The FT-IR spectra of rGO consist of apparent peaks at 1623 and 1556 cm^{-1} corresponding to the aromatic C=C stretch, whereas the peak at 1234 cm^{-1} represents the C=O, and epoxy C−O peaks are not completely reduced. The FT-IR spectra of ZrO$_2$@rGO and the pure ZrO$_2$ particles are presented in Figure 1B. The strong absorption peaks at 3420, 1631, and 1558 cm^{-1} of pure ZrO$_2$ are owing to stretching vibrations of the stretching υ (−OH) and bending δ (−OH) of coordinated water or the water molecules retained in the ZrO$_2$ matrix. The FT-IR spectra of ZrO$_2$@rGO consist of apparent peaks at 1577 and 1686 cm^{-1} corresponding to the aromatic C=C stretch, whereas the weak peak at 1224 cm^{-1} represents the epoxy C=O or C=O peaks, which are not completely reduced in rGO. The chemical composition of ZrO$_2$@rGO before and after Re(VII) sorption was analyzed by XPS (Figure 1C). The peaks

corresponding to Zr 3d, O 1s, C 1s, and Re 4f are identified in the scan spectrum clearly. The presence of Re 4f in the resultant sample further confirms Re(VII) sorption onto ZrO$_2$@rGO. The expatiation of all the XPS fitting results, including peak position and assignment, is discussed in the XPS Analyses section.

The TGA curves of raw ZrO$_2$ and ZrO$_2$@rGO (800:90) are shown in Figure 2A. The mass loss below 200 °C may be due to the mass loss of water evaporation. The first mass losses of ZrO$_2$ and ZrO$_2$@rGO were calculated to be 4.43% and 7.49%, respectively. The second mass loss process appearance in ZrO$_2$ may be owing to the crystal water doping from the synthetic process or in the interlayer. The second mass loss of ZrO$_2$@rGO ascribes to the oxidative decomposition of the rGO framework. All results above confirm that ZrO$_2$ has been decorated on the surface of rGO successfully with 66.9% of the content approximately.

The N$_2$ adsorption/desorption isotherms of ZrO$_2$ and ZrO$_2$@rGO are shown in Figure 2B and Figure S4A. The N$_2$−BET surface areas of ZrO$_2$@rGO(800:90) and ZrO$_2$ were calculated to be 272.73 and 25.90 (m^2/g), respectively. The N$_2$−BET surface areas of the rGO and ZrO$_2$@rGO composites with the mass ratios of ZrO$_2$ to GO of 200:90, 400:90, and 1600:90 were calculated to be 296.00, 18.47, 40.29, and 223.90 (m^2/g), respectively. The BET surface area of ZrO$_2$@rGO is higher than ZrO$_2$ and therefore provides more sorption sites. With the increasing mass ratios of ZrO$_2$ to GO, the BET surface area of ZrO$_2$@rGO increases first and then decreases. From the distributions of pore diameters of ZrO$_2$ and ZrO$_2$@rGO (Figure 2C and Figure S4B), ZrO$_2$@rGO possesses more large amounts of macropores (>500 Å) in its structures than
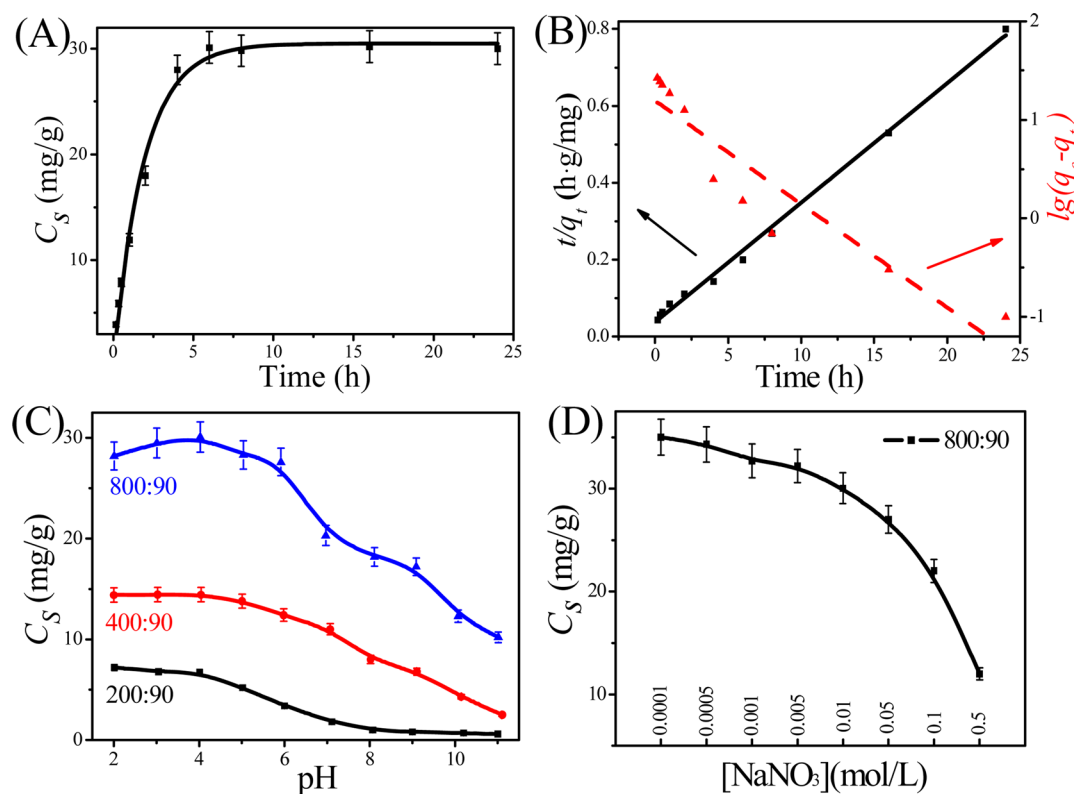
Figure 3. (A) Effect of contact time on Re(VII) sorption onto ZrO$_2$@rGO(800:90): pH 4.0 ± 0.1, m/V = 0.1 g/L, $C_{[Re(VII)]initial}$ = 10.00 mg/L, and T = 293 K. (B) Fitting of the pseudo-first-order (imaginary line) and pseudo-second-order (solid line) kinetic models. (C) Effect of pH on Re (VII) sorption to different mass ratio ZrO$_2$@rGO: m/V = 0.1 g/L, $C_{[Re(VII)]initial}$ = 10.00 mg/L, I = 0.01 mol/L NaNO$_3$, and T = 293 K. (D) Effect of ionic strength on Re(VI) sorption on ZrO$_2$@rGO(800:90): pH 4.0 ± 0.1 and m/V = 0.1 g/L.

ZrO$_2$. Furthermore, there are micropores (<20 Å) and mesopores (20−500 Å) in the structures of ZrO$_2$@rGO. The growth of ZrO$_2$ crystals on the rGO surface will block the rGO mesopores, leading to the amounts of mesopores decreasing. However, with the ratio of ZrO$_2$ increasing, new mesopores will be formed between ZrO$_2$ particles growing on the surface of rGO. The porous structure favors the rapid diffusion of sorbate by providing interconnected and low-resistance channels for the sorbent, which is beneficial for the sorption.

Zeta potential (ZP) values of GO, rGO, ZrO$_2$, and ZrO$_2$@rGO were measured and are shown in Figure 2D. The surface of GO and rGO is negatively charged within the pH range from 3.0 to 11.0, while the ZP values of rGO is higher than GO. It can be explained that GO with abundant functional groups is difficultly protonated and positively charged, and the reduction of GO to rGO reduces the functional groups. The positively charged ZrO$_2$ is easily decorated on the negatively charged surface of rGO because of the electrostatic attraction. The ZrO$_2$@rGO surface is positively charged ranging from pH 1.5 to 6.2 due to the positively charged ZrO$_2$ decorated on the rGO surface. The point of zero charge (pHpzc) value of ZrO$_2$@rGO is 6.2. Such considerations that predict the impact of pH on anion Re(VII) to ZrO$_2$@rGO are evaluated later.

Sorption Kinetics. Figure 3A shows the impact of shaking time on the sorption of anion Re(VII) on ZrO$_2$@rGO. The sorption of the Re(VII) anion on ZrO$_2$@rGO increases quickly at first; after that, it remains stable with the rising time. The shaking time in all the later experiments is fixed 24 h to ensure the Re(VII) anion sorption process complete equilibrium. The kinetics sorption was described by the pseudo-first-order (eq 1) and pseudo-second order (eq 2) rate equations:[32,33]

$$lg(q_e - q_t) = lg(q_e) - \frac{k_1 \times t}{2.303} \tag{2}$$

$$\frac{t}{q_t} = \frac{1}{2k'q_e^2} + \frac{1}{q_e}t \tag{3}$$

where q_e (mg/g) and q_t (mg/g) are the sorption capacities at equilibrium and time t (h), respectively, k_1 (h^{-1}) is the rate constant of first-order sorption, and k_2 (g/(mg h)) is the one of the second-order reaction. The fitting results of pseudo-first-order (plot of $lg(q_e - q_t)$ versus t (h)) and pseudo-second-order (plot of t/q_t versus t (h)) are shown in Figure 3B. The relevant parameters are shown in Table S1. The correlation coefficient of the pseudo-second-order rate equation is 0.997 (pseudo-first-order: 0.863), which confirms that the rate equation of pseudo-second-order fits well the sorption kinetics of Re(VII).[34−36]

Effect of Solution's pH and Anion. The solution's pH impacts the surface complexation process through changing the electric charge of the sorbate and sorbent surface.[10] The sorbent surface will be positively charged once the pH of the solution is lower than the pH$_{PZC}$ (point of zero charge). On the contrary, when the pH is higher than the pH$_{PZC}$ of the sorbent, the sorbent surface will be negatively charged. The effect of the solution's pH on the sorption of Re(VII) onto ZrO$_2$@rGO with the mass ratios of ZrO$_2$ to GO of 200:90, 400:90, 800:90, and 1600:90 was studied from pH 2.0 to 11.0. As shown in Figure 3C and D, the sorption of Re(VII) depends strongly on the extra anion strength and the solution's pH. The sorption on the different mass ratios of ZrO$_2$@rGO decreases slow at pH values from 2.0 to 4.0 and then decreases sharply with the

Table 1. Values of Thermodynamic Parameters for Re(VII) Sorption on ZrO$_2$@rGO

	Langmuir			Freundlich			D-R		
T (K)	C_{smax} (mg/g)	b (L/mg)	R^2	K_F (mg^{1-n} L^n/g)	n	R^2	β (mg^2/kJ^2)	C_{smax} (mg/g)	R^2
293	43.55	0.210	0.987	11.15	0.410	0.885	1.75×10^{-6}	34.24	0.975
313	47.39	0.877	0.999	24.47	0.224	0.863	4.46×10^{-7}	43.37	0.976
333	62.50	1.345	0.999	50.77	0.060	0.830	1.37×10^{-7}	58.66	0.980

increase in pH value from 4.0. This phenomenon is similar to the trend of the ZP's changing of ZrO$_2$@rGO. From pH 2.0 to 4.0, ZrO$_2$@rGO shows the largest sorption capacity of Re(VII). Therefore, the experiments of sorption kinetics and isotherms were conducted at pH 4.0 in this study. The pH$_{pzc}$ of ZrO$_2$@rGO with different ratios is increasing from 4.8 to 6.0, indicating that at pH below 4.8 the ZrO$_2$@rGO is carrying positive charges because of the surface protonation. The electrostatic attraction probably plays an significant impact on the sorption process of Re(VII) onto ZrO$_2$@rGO. The perrhenate anions (ReO$_4^-$) predominate over almost the entire pH range from 0 to14 under solution conditions.[4]

When pH ranges from 2.0 to 4.0, the surface of ZrO$_2$@rGO is positively charged and keeps decreasing slowly. So, the electrostatic attraction between ReO$_4^-$ and ZrO$_2$@rGO decreases very slowly, leading to the gradual decrease in Re(VII) sorption.

Re(VII) sorption on the ZrO$_2$@rGO can be through electrostatic attraction and surface complexation

$$\equiv SOH_2^+ + ReO_4^- \rightarrow \equiv SOH_2^+ \cdots ReO_4^- \tag{5}$$
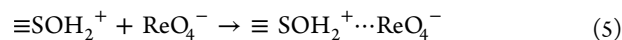
However, from pH > 4.0, the concentration of ReO$_4^-$ increases and the positive charge of ZrO$_2$@rGO reduces. The electrostatic attraction force between ReO$_4^-$ and ZrO$_2$@rGO gradually was weakened, leading to reduction of Re(VII) sorption on ZrO$_2$@rGO.

From pH above 6.0, ZrO$_2$@rGO(800:90) is negatively charged because of the deprotonating process of competitive sorption of hydroxyl on the surface. At the same time, most Re(VII) is in the form of ReO$_4^-$ anions. ZrO$_2$@rGO and Re(VII) ions will repel each other through the charge repulsion. The increase in pH probably results in increasing the electrostatic repulsive force and the concentration of OH$^-$, which decreases the sorption capacity of Re(VII) on ZrO$_2$@rGO. The repulsion force will increase with the rise in the solution's pH. This is the reason why the sorption capacity decreased extremely low from pH 4.0 to 11.0 gradually. The same phenomenon was also discovered in the sorption process of Re(VII) onto the modified nano-Al$_2$O$_3$,[9] and the dye (negative electricity) adsorption on PANI/α-ZrP had the same consequence.[13]

The interaction between ZrO$_2$@rGO and the extra ions in the solution system is also studied. The surface of ZrO$_2$@rGO is positively charged and has lower adsorption capacity to cations at pH < 6.2 due to the electrostatic repulsion. Therefore, the effect of cations was neglected. The sorption of Re(VII) may be affected by extra anions in solution from two modalities: (1) the competing ion-exchange with extra anions (NO$_3^-$) and (2) the general impact of the "saline effect" and "ionic atmosphere" caused by all the extra ions (Na$^+$, OH$^-$, and all other), while ignoring the possible sorption on the surface. Here, the impact of NO$_3^-$ concentration on the sorption mainly comes from the competing sorption effect.[10] The sorption of the Re(VII) anion onto ZrO$_2$@rGO is the highest in the solution without extra NO$_3^-$, while the lowest in the

solution with 0.5 mol/L NO$_3^-$. With the rise in NO$_3^-$concentration, the sorption capacity of Re(VII) reduces gradually. The above results make it clear that the outer-sphere complexation contributes to Re(VII) sorption on ZrO$_2$@rGO.[21,37]

Sorption Isotherms. The sorption isotherms of Re(VII) at 293, 313, and 333 K on ZrO$_2$@rGO (800:90) are illustrated in Figure S5A. The sorption capacity of Re(VII) on ZrO$_2$@rGO increases with the temperature rising, which demonstrates that higher temperature favors the sorption of Re(VII). To better understand the sorption mechanism and quantify the sorption data, the Langmuir, Freundlich, and D−R models (described in the Supporting Information) are used to describe the experimental data.

Figure S5B−D show the simulated results. The relative parameters calculated from the three sorption models are shown in Table 1. Through comparing the correlation coefficients, we find that the Langmuir model describes the experimental data better than the other two sorption models. The values of C_{smax} calculated from the Langmuir model at T = 333 K for Re(VII) sorption on ZrO$_2$@rGO are the highest, while calculated at T = 293 K are the lowest, indicating that the sorption process of Re(VII) is enhanced by the rising temperature.

The thermodynamic parameters (ΔH^0, ΔS^0, and ΔG^0) for Re(VII) sorption on ZrO$_2$@rGO are calculated from the temperature-dependent sorption isotherms. The Gibbs free energy change (ΔG^0) is calculated by the following equation:

$$\Delta G^\circ = -RT \ln K^0 \tag{10}$$

where K^0 is the constant of sorption equilibrium. Values of ln K^0 are calculated by plotting in K_d versus C_e and extrapolating C_e to zero (Figure S6A). Its intercept with the vertical axis gives the value of ln K_0.

$$\ln(K^0) = \frac{\Delta S^\circ}{R} - \frac{\Delta H^\circ}{RT} \tag{11}$$

where the R is the constant of the universal gas (8.314 J mol K) and T is the temperature in Kelvin. By plotting ln K^0 versus $1/T$ (Figure S6B), we can obtain the $-\Delta H^0/R$ value from the slope and the $\Delta S^0/R$ value from the intercept.

The positive value of ΔH^0 (Table S2) proves the endothermic sorption process. A possible reason for the positive value of ΔH^0 is that the Re(VII) anion can be dissolved in the water well, while the hydration sheath from anion Re(VII) needs to be broken before it is sorbed on the ZrO$_2$@rGO surface.

The process of dehydration needs energy to break the hydration sheath, which will be promoted at higher temperature. The energy surpasses the anion sorption exothermicity on the solid surface.[10,38] This hypothesis proves that the endothermcity in the process of desolvation is higher than the sorption enthalpy to some extent. The negative change of ΔG^o indicates a spontaneous process. The values of ΔG^0 decrease
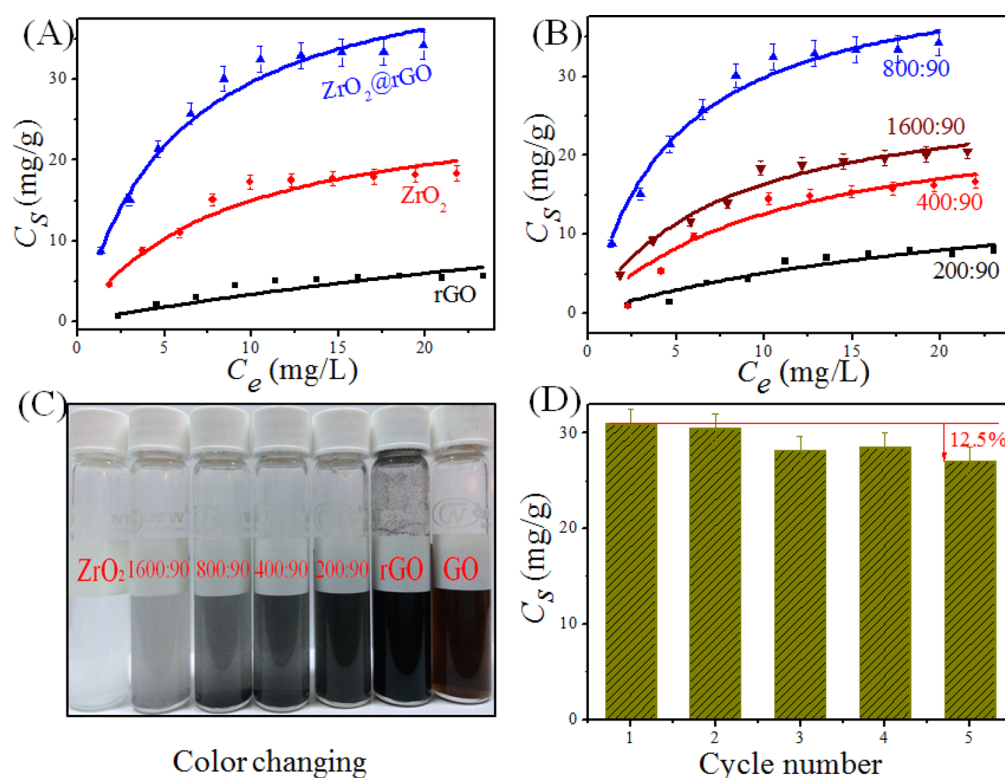
Figure 4. (A) Sorption isotherms of Re(VII) sorption onto ZrO_2, rGO, and ZrO_2@rGO (800:90):pH 4.0 ± 0.1, I = 0.01 mol/L $NaNO_3$, m/V = 0.1 g/L, and T = 293 K. (B) Sorption isotherms of Re(VII) sorption on ZrO_2@rGO with mass ratios ZrO_2 to GO of 200:90, 400:90, 800:90, and 1600:90. (C) Color change of the sorbent we used in this work. (D) Recycling of ZrO_2@rGO in the removal of Re(VII).

following the increasing temperature, which is more beneficial to the sorption process at higher temperature. At higher temperature, anions are easily desolvated, and then, the process of sorption becomes more easy. The sorption process of Re(VII) onto ZrO_2@rGO is endothermic and spontaneous.[24,39] The positive value of entropy change ($\Delta S°$) indicates some structural changes of sorbate and sorbent during the sorption process, leading to the disorderness of the solid−solution systems. What is more, the Re(VII) anion is encircled by a strong bound hydration layer of highly ordered water molecules in the solution. While the Re(VII) anion comes into close interaction with the hydration surface of the sorbent, the ordered water molecules in the two hydration layers compel and disturb each other, which increases the $\Delta S°$ of the water molecule.[10,40]

Figure 4A shows the typical isotherms of Re(VII) sorption on ZrO_2, rGO, and ZrO_2@rGO. ZrO_2@rGO showed a more intensive sorption capability of Re(VII) than individual ZrO_2 (24.85 mg/g) and rGO (9.50 mg/g) because of its more positively charged active binding sites than rGO and higher specific surface area than ZrO_2. The positively charged ZrO_2 and high BET surface area of rGO provided more active binding sites, which was expected to explain the high Re(VII) sorption on ZrO_2@rGO.[21] Table S3 shows the q_{max} values of anion Re(VII) on other sorbents. The sorption capacity of ZrO_2@rGO (43.55 mg/g) is the highest compared to the former reported sorbents. For example, the sorption capacity of modified BA is 37.20 mg/g,[6] the modified nanoaluminum oxide is 1.85 mg/g,[9] and so on.

As a comparison, ZrO_2@rGO composites with mass ratios of ZrO_2 to GO of 200:90, 400:90, 800:90, and 1600:90 were prepared. From Figure 4B, the sorption of Re(VII) on ZrO_2@

rGO composites with the mass ratio of ZrO_2 to GO of 200:90 is the lowest, and with increasing ZrO_2, the content of sorption increases. This is due to the sorption capacities from the positively charged ZrO_2 through electrostatic attraction. However, with an increase in mass ratios from 800:90 to 1600:90, the sorption capacities decrease because much ZrO_2 not only occupied active sites of rGO but also decreased the BET specific surface area. Futhermore, rGO has a limited load capacity of ZrO_2. Thus, with an increasing content of ZrO_2, some ZrO_2 cannot successfully decorate on the surface of rGO. However, it will form individual ZrO_2, and therefore, the sorption capacity decreases.

Figure 4C shows the color change of the sorbent. The color of GOs is claybank. Through hydrothermal reduction, claybank GOs turn into black rGO, while the color of ZrO_2 is milky. The color of different ratios of ZrO_2@rGO becomes shallow gradually with the increase in the ratio of ZrO_2.

The recycling of ZrO_2@rGO (200:90) was also studied. In brief, the sorbent after Re(VII) sorption was rinsed with 6 mL of NaOH dilute solution (0.05 mol/L). Then, the suspension solution was centrifuged after a day, and the solid was dispersed with 6 mL of dilute HNO_3 (0.05 mol/L) and then rinsed with Milli-Q water. After centrifugation, ZrO_2@rGO was dried at −60 °C by vacuum freeze-drying and reused.[10] Figure 4D shows that the sorption of Re(VII) on ZrO_2@rGO decreases slightly with the increase in recycling times. However, the reduction is less than 5% after recycling five times, showing the good reusability of ZrO_2@rGO.

XPS Analyses. The chemical composition of ZrO_2@rGO before and after the sorption of Re(VII) was measured by XPS. Table S4 shows the XPS details of ZrO_2@rGO before and after Re(VII) sorption. As shown in Figures 1C and 5 of the scan
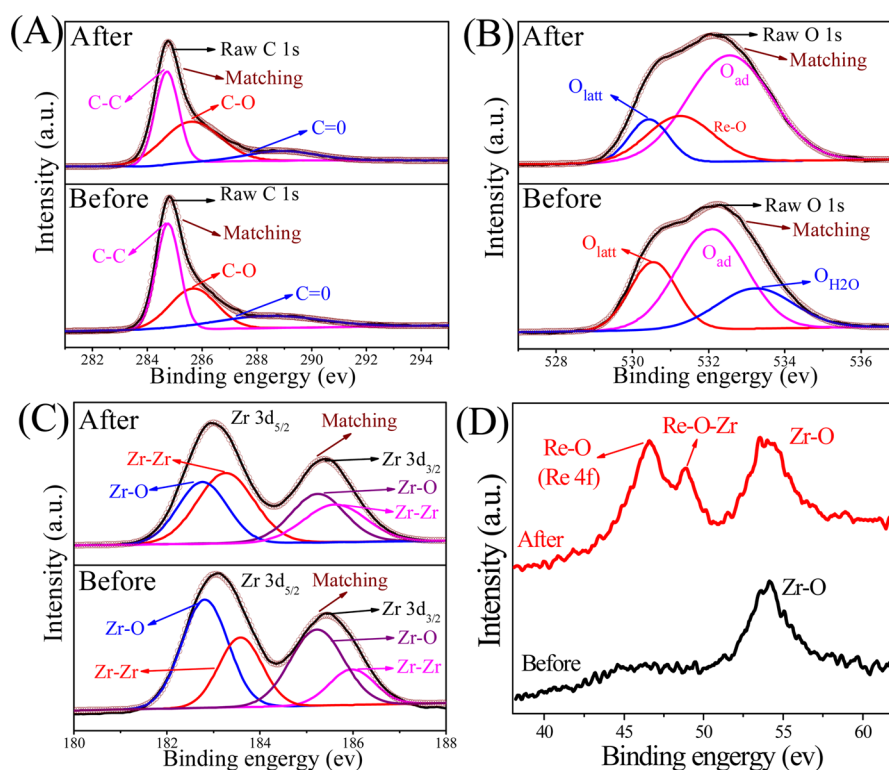
Figure 5. XPS survey spectra of (A) C 1s, (B) O 1s, (C) Zr 3d, and (D) Re 4f.

spectra, there are the obviously peaks corresponding to C 1s, O 1s, Zr 3d, and Re 4f. The presence of Re(VII) in the resultant sample further confirms Re(VII) sorption onto ZrO_2@rGO. The peak at a binding energy of 284.77 eV is assigned to C 1s (Figure 5A), and no obvious change of C 1s has been identified before and after Re(VII) sorption.

From Figure 5B, the O_{latt} (lattice oxygen: C—O and C—O—Zr) peak strength decreased after Re(VII) sorption on the surface, and there is a new Re—O peak appearing, which is primarily attributed to the fact that Re(VII) is bonded in O_{Re}—Zr. The binding energy of O_{ad} (adsorb oxygen: O—Zr—O) increased from 532.10 to 532.55 eV, indicating that Re(VII) formed complexes with the surface oxygen-containing ZrO_2.

As displayed in Figure 5C, the peak of Zr 3d can be decomposed into four peaks. The peaks at approximately 182.82 and 185.23 eV are attributed to Zr—O bonds, and the peaks at approximately 183.58 and 185.98 eV are the metallic Zr bonds (Zr—Zr). In addition, the strength of the Zr—O peaks reduce after Re(VII) sorption because Re(VII) is bonded on ZrO_2. The core level shifts indicated an electron transfer in the valence band involving the reaction between Re(VII) and ZrO_2 on the surface of rGO. This finding indicates that the Zr—O site plays a dominating role in the sorption of Re(VII). The two peaks around 46.51 eV are attributed to Re 4f. The appearance of the Re 4f peak in Figure 5D indicates that Re(VII) is sorbed on ZrO_2@rGO.

DFT Calculations. To distinguish the O atoms of ReO_4^- from that of ZrO_2, we name the O atoms of ReO_4^- as O_{Re}. Re(VII) is sorbed at surface Zr sites through an O_{Re}—Zr bond, as shown in Figure 6A and B; this is found to be the stable molecular adsorption structure (one oxygen of Re(VII) down). For the t-ZrO_2 (111) plane (as shown in Figure 6A), the adsorption energy is 3.87 eV, higher than the m-ZrO_2 (111) plane (1.26 eV), and the bond length of O—Zr is 2.06 Å. For
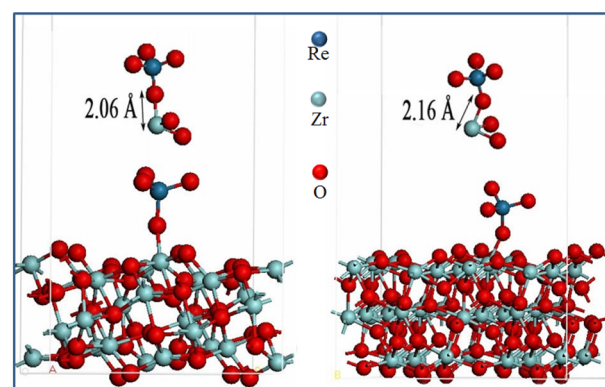

Figure 6. Optimized (A) t-ZrO_2 (111) plane and (B) m-ZrO_2 (111) plane slab models for Re(VII) sorption. O atoms are red. Zr atoms are blue. Re atoms are gray. The actual sorption sites as part of the slab are shown above sorbed Re(VII) onto the plane slabs.

the m-ZrO_2 (111) plane (as shown in Figure 6B), the bond length of O—Zr is 2.16 Å.

In order to further understand the molecular adsorption modes, projected density of states (PDOS) analyses were carried out. Figure S7 shows the sorption of the O_{Re}—Zr configuration for O in Re(VII) and closed surface Zr. As illustrated in Figure S7a for t-ZrO_2, the Zr d and s orbitals located in the range from −5 and 0 eV overlap with the O orbitals to favor the charge transfer leading to the ionic species, contributing to stabilize the structure.

Four oxygen atoms surround the Re atoms, and the Re atoms cannot easily interact with the surface zirconium atoms directly; therefore, the sorption occurred by the O_{Re}—Zr bond. The difference of distribution of oxygen on the surfaces for t-ZrO_2 and m-ZrO_2 may have an influence on the adsorption energy,

leading to the adsorption energy of t-ZrO_2 being higher than m-ZrO_2.

CONCLUSIONS

In this study, ZrO_2@rGO was fabricated via a hydrothermal method. Re(VII) sorption kinetics on the ZrO_2@rGO can be fitted by the pseudo-second-order rate equation well. The thermodynamic parameters imply that Re(VII) sorption on ZrO_2@rGO is spontaneous and endothermic. ZrO_2@rGO has a maximum Re(VII) sorption capacity of 43.55 mg/g and exhibits enhanced sorption capacity for Re(VI) in comparison with bare ZrO_2 or rGO. The mechanism of Re(VII) sorption on ZrO_2@rGO could be briefly illustrated as follows: Re(VII) sorption on the ZrO_2@rGO is dependent on the solution's pH and extra ionic strength, indicating that the electrostatic attraction and outer-sphere complexation play a dominating impact on Re(VII) sorption onto ZrO_2@rGO. On the basis of DFT calculations, O_{Re}−Zr bonds on the surface of the monoclinic ZrO_2 plane (m-ZrO_2) (111) plane and tetragonal ZrO_2 (t-ZrO_2) (111) plane were formed when Re(VII) sorbs. These results are significant for evaluating the sorption capacity of Re(VII) on ZrO_2@rGO. Furthermore, we can infer that Tc(VII) has a similar property of sorption on ZrO_2@rGO.

ASSOCIATED CONTENT

ⓢ Supporting Information

The Supporting Information is available free of charge on the ACS Publications website at DOI: 10.1021/acssusche-meng.6b02317.

> Characterization, sorption experiments, kinetic and thermodynamic parameters, comparison of the maximum sorption capacity, XPS data, and projected density of states. (PDF)

AUTHOR INFORMATION

Corresponding Authors

*Tel: +86-551-65592788. Fax: +86-551-65591310. E-mail: tanxl@ipp.ac.cn (X.L. Tan).
*E-mail: tahaksag@yahoo.com (T. Hayat).
*Tel: +86-551-65592788. Fax: +86-551-65591310. E-mail: clchen@ipp.ac.cn (C.L. Chen).

ORCID ⓘ

Changlun Chen: 0000-0002-7986-8077

Notes

The authors declare no competing financial interest.

ACKNOWLEDGMENTS

REFERENCES

(1) Boggs, M. A.; Minton, T.; Dong, W.; Lomasney, S.; Islam, M. R.; Gu, B.; Wall, N. A. Interactions of Tc(IV) with humic substances. *Environ. Sci. Technol.* **2011**, *45*, 2718−2724.

(2) Lecina, J.; Cortes, P.; Llagostera, M.; Piera, C.; Suades, J. New Rhenium Complexes with ciprofloxacin as useful models for understanding the properties of Tc-99 m-ciprofloxacin radiopharma-ceutical. *Bioorg. Med. Chem.* **2014**, *22*, 3262−3269.

(3) Sheng, G. D.; Tang, Y. N.; Linghu, W. S.; Wang, L. J.; Li, J. X.; Li, H.; Wang, X. K.; Huang, Y. Y. Enhanced immobilization of ReO_4^- by nanoscale zerovalent iron supported on layered double hydroxide via an advanced XAFS approach: Implications for TcO_4^- sequestration. *Appl. Catal., B* **2016**, *192*, 268−276.

(4) Darab, J. G.; Smith, P. A. Chemistry of technetium and rhenium species during low-level radioactive waste vitrification. *Chem. Mater.* **1996**, *8*, 1004−1021.

(5) Seo, S. Y.; Choi, W. S.; Yang, T. J.; Kim, M. J.; Tran, T. Recovery of rhenium and molybdenum from a roaster fume scrubbing liquor by adsorption using activated carbon. *Hydrometallurgy* **2012**, *129-130*, 145−150.

(6) Xiong, Y.; Xu, J.; Shan, W.; Lou, Z.; Fang, D.; Zang, S.; Han, G. A New Approach for rhenium(VII) recovery by using modified brown algae laminaria japonica sorbent. *Bioresour. Technol.* **2013**, *127*, 464−472.

(7) Hu, H.; Jiang, B.; Zhang, J.; Chen, X. Adsorption of perrhenate ion by bio-char produced from acidosasa edulis shoot shell in aqueous solution. *RSC Adv.* **2015**, *5*, 104769−104778.

(8) Li, J.; Chen, C. L.; Zhang, R.; Wang, X. K. Reductive immobilization of Re(VII) by graphene modified nanoscale zero-valent iron particles using a plasma technique. *Sci. China: Chem.* **2016**, *59*, 150−158.

(9) Zhang, L.; Jiang, X. Q.; Xu, T. C.; Yang, L. J.; Zhang, Y. Y.; Jin, H. J. Sorption characteristics and separation of rhenium ions from aqueous solutions using modified nano-Al_2O_3. *Ind. Eng. Chem. Res.* **2012**, *51*, 5577−5584.

(10) Gao, Y.; Chen, C. L.; Chen, H.; Zhang, R.; Wang, X. K. Synthesis of a novel organic−inorganic hybrid of polyaniline/titanium phosphate for Re(VII) removal. *Dalton. Trans.* **2015**, *44*, 8917−8925.

(11) Shan, W.; Fang, D.; Zhao, Z.; Shuang, Y.; Ning, L.; Xing, Z.; Xiong, Y. Application of orange peel for adsorption separation of molybdenum(VI) from Re-containing industrial effluent. *Biomass Bioenergy* **2012**, *37*, 289−297.

(12) Xiong, Y.; Wang, H.; Lou, Z.; Shan, W.; Xing, Z.; Deng, G.; Wu, D.; Fang, D.; Biswas, B. K. Selective adsorption of molybdenum(VI) from Mo−Re bearing effluent by chemically modified astringent persimmon. *J. Hazard. Mater.* **2011**, *186*, 1855−1861.

(13) Wang, L.; Wu, X. L.; Xu, W. H.; Huang, X. J.; Liu, J. H.; Xu, A. W. Stable organic−inorganic hybrid of polyaniline/α-zirconium phosphate for efficient removal of organic pollutants in water environment. *ACS Appl. Mater. Interfaces* **2012**, *4*, 2686−2692.

(14) Swain, S.; Mishra, S.; Sharma, P.; Patnaik, T.; Singh, V.; Jha, U.; Patel, R.; Dey, R. Development of a new inorganic−organic hybrid ion-exchanger of zirconium(IV)−propanolamine for efficient removal of fluoride from drinking water. *Ind. Eng. Chem. Res.* **2010**, *49*, 9846−9856.

(15) Sanchez, C.; Julian, B.; Belleville, P.; Popall, M. Applications of hybrid organic−inorganic nanocomposites. *J. Mater. Chem.* **2005**, *15*, 3559−3592.

(16) Takei, T.; Kobayashi, Y.; Hata, H.; Yonesaki, Y.; Kumada, N.; Kinomura, N.; Mallouk, T. E. Anodic electrodeposition of highly oriented zirconium phosphate and polyaniline-intercalated zirconium phosphate films. *J. Am. Chem. Soc.* **2006**, *128*, 16634−16640.

(17) Ntim, S. A.; Mitra, S. Adsorption of Arsenic on multiwall carbon nanotube−zirconia nanohybrid for potential drinking water purifica-tion. *J. Colloid Interface Sci.* **2012**, *375*, 154−159.

(18) Hristovski, K. D.; Westerhoff, P. K.; Crittenden, J. C.; Olson, L. W. Arsenate removal by nanostructured ZrO_2 spheres. *Environ. Sci. Technol.* **2008**, *42*, 3786−3790.

(19) Chen, D.; Cao, L.; Hanley, T. L.; Caruso, R. A. Facile synthesis of monodisperse mesoporous zirconium titanium oxide microspheres with varying compositions and high surface areas for heavy metal ion sequestration. *Adv. Funct. Mater.* **2012**, *22*, 1966−1971.

(20) Rodrigues, L. A.; Maschio, L. J.; da Silva, R. E.; da Silva, M. L. C. P. Adsorption of Cr(VI) from aqueous solution by hydrous zirconium oxide. *J. Hazard. Mater.* **2010**, *173*, 630−636.

(21) Luo, J.; Luo, X.; Crittenden, J.; Qu, J.; Bai, Y.; Peng, Y.; Li, J. Removal of antimonite (Sb(III)) and antimonate (Sb(V)) from aqueous solution using carbon nanofibers that are decorated with zirconium oxide (ZrO_2). *Environ. Sci. Technol.* **2015**, *49*, 11115−11124.

(22) Cui, H.; Su, Y.; Li, Q.; Gao, S.; Shang, J. K. Exceptional arsenic (III,V) removal performance of highly porous, nanostructured ZrO_2 spheres for fixed bed reactors and the full-scale system modeling. *Water Res.* **2013**, *47*, 6258−6268.

(23) Tel, H.; Altas, Y.; Eral, M.; Sert, S.; Cetinkaya, B.; Inan, S. Preparation of ZrO_2 and ZrO_2−TiO_2 microspheres by the Gol−Gel method and an experimental design approach to their strontium adsorption behaviours. *Chem. Eng. J.* **2010**, *161*, 151−160.

(24) Zhang, Q. R.; Du, Q.; Jiao, T. F.; Teng, J.; Sun, Q. N.; Peng, Q. M.; Chen, X. Q.; Gao, F. M. Accelerated sorption diffusion for Cu(II) retention by anchorage of nano-zirconium dioxide onto highly charged polystyrene material. *Sci. Rep.* **2015**, *5*, 10646.

(25) Zhao, J. C.; Ding, X. G.; Meng, C.; Ren, C. R.; Fu, H. Q.; Yang, H. Adsorption and immobilization of actinides using novel SiO_2-ZrO_2-calcium alginate aerogels from high level liquid waste. *Prog. Nucl. Energy* **2015**, *85*, 713−718.

(26) Zhao, G. X.; Li, J. X.; Ren, X. M.; Chen, C. L.; Wang, X. K. Few-layered graphene oxide nanosheets as superior sorbents for heavy metal ion pollution management. *Environ. Sci. Technol.* **2011**, *45*, 10454−10462.

(27) Kresse, G.; Hafner, J. Ab initio molecular dynamics for liquid metals. *Phys. Rev. B: Condens. Matter Mater. Phys.* **1993**, *47*, 558−561.

(28) Kresse, G.; Hafner, J. Ab Initio Molecular-dynamics simulation of the liquid-metal-amorphous-semiconductor transition in germanium. *Phys. Rev. B: Condens. Matter Mater. Phys.* **1994**, *49*, 14251−14269.

(29) Blöchl, P. E. Projector augmented-wave method. *Phys. Rev. B: Condens. Matter Mater. Phys.* **1994**, *50*, 17953−17979.

(30) Perdew, J. P.; Burke, K.; Ernzerhof, M. Generalized gradient approximation made simple. *Phys. Rev. Lett.* **1996**, *77*, 3865−3868.

(31) Kresse, G.; Joubert, D. From ultrasoft pseudopotentials to the projector augmented-wave method. *Phys. Rev. B: Condens. Matter Mater. Phys.* **1999**, *59*, 1758−1775.

(32) Ho, Y. S.; McKay, G. Pseudo-second order model for sorption processes. *Process Biochem.* **1999**, *34*, 451−465.

(33) Hu, J.; Shao, D. D.; Chen, C. L.; Sheng, G. D.; Ren, X. M.; Wang, X. K. Removal of 1-naphthylamine from aqueous solution by multiwall carbon nanotubes/iron oxides/cyclodextrin composite. *J. Hazard. Mater.* **2011**, *185*, 463−471.

(34) Chen, C. L.; Wang, X. K. Adsorption of Ni(II) from aqueous solution using oxidized multiwall carbon nanotubes. *Ind. Eng. Chem. Res.* **2006**, *45*, 9144−9149.

(35) Li, J.; Zhang, S. W.; Chen, C. L.; Zhao, G. X.; Yang, X.; Li, J. X.; Wang, X. K. Removal of Cu(II) and fulvic acid by graphene oxide nanosheets decorated with Fe_3O_4 nanoparticles. *ACS Appl. Mater. Interfaces* **2012**, *4*, 4991−5000.

(36) Yang, X.; Chen, C. L.; Li, J. X.; Zhao, G. X.; Ren, X. M.; Wang, X. K. Graphene oxide-iron oxide and reduced graphene oxide-iron oxide hybrid materials for the removal of organic and inorganic pollutants. *RSC Adv.* **2012**, *2*, 8821−8826.

(37) Wen, T.; Wu, X. L.; Tan, X. L.; Wang, X. K.; Xu, A. W. One-pot synthesis of water-swellable Mg−Al layered double hydroxides and graphene oxide nanocomposites for efficient removal of As(V) from aqueous solutions. *ACS Appl. Mater. Interfaces* **2013**, *5*, 3304−3311.

(38) Gong, J.; Liu, T.; Wang, X.; Hu, X.; Zhang, L. Efficient removal of heavy metal ions from aqueous systems with the assembly of anisotropic layered double hydroxide nanocrystals@carbon nanosphere. *Environ. Sci. Technol.* **2011**, *45*, 6181−6187.

(39) Yang, S. B.; Hu, J.; Chen, C. L.; Shao, D. D.; Wang, X. K. Mutual effects of Pb(II) and humic acid adsorption on multiwalled carbon nanotubes/polyacrylamide composites from aqueous solutions. *Environ. Sci. Technol.* **2011**, *45*, 3621−3627.

(40) Geckeis, H.; Rabung, T.; Manh, T. N.; Kim, J.; Beck, H. Humic colloid-borne natural polyvalent metal ions: dissociation experiment. *Environ. Sci. Technol.* **2002**, *36*, 2946−2952.